Available online at www.sciencedirect.com
ScienceDirect
Geochimica et Cosmochimica Acta 73 (2009) 962–976
Geochimica et Cosmochimica Acta
www.elsevier.com/locate/gca

Bioreduction of hematite nanoparticles by the dissimilatory iron reducing bacterium *Shewanella oneidensis* MR-1

Saumyaditya Bose [a,1], Michael F. Hochella Jr. [a], Yuri A. Gorby [b], David W. Kennedy [c], David E. McCready [c], Andrew S. Madden [d], Brian H. Lower [e,*]

[a] *Center for NanoBioEarth, Department of Geosciences, Virginia Tech, Blacksburg, VA 24061, USA*
[b] *J. Craig Venter Institute, 11149 North Torrey Pines Road, La Jolla, CA 92037, USA*
[c] *Pacific Northwest National Laboratory, Richland, WA 99352, USA*
[d] *School of Geology and Geophysics, University of Oklahoma, Norman, OK 73019, USA*
[e] *School of Environment and Natural Resources, The Ohio State University, Columbus, OH 43210, USA*

Received 27 December 2007; accepted in revised form 11 November 2008; available online 7 January 2009

Abstract

We examined the reduction of different size hematite (α-Fe_2O_3) nanoparticles (average diameter of 11, 12, 30, 43, and 99 nm) by the dissimilatory iron reducing bacteria (DIRB), *Shewanella oneidensis* MR-1, to determine how *S. oneidensis* MR-1 may utilize these environmentally relevant solid-phase electron acceptors. The surface-area-normalized-bacterial Fe(III) reduction rate for the larger nanoparticles (99 nm) was one order of magnitude higher than the rate observed for the smallest nanoparticles (11 nm). The Fe(III) reduction rates for the 12, 30, and 43 nm nanoparticles fell between these two extremes. Whole-cell TEM images showed that the mode of Fe_2O_3 nanoparticle attachment to bacterial cells was different for the aggregated, pseudo-hexagonal/irregular and platey 11, 12, and 99 nm nanoparticles compared to the non-aggregated 30 and 43 nm rhombohedral nanoparticles. Due to differences in aggregation, the 11, 12, and 99 nm nanoparticles exhibited less cell contact and less cell coverage than did the 30 and 43 nm nanoparticles. We hypothesize that *S. oneidensis* MR-1 employs both indirect and direct mechanisms of electron transfer to Fe(III)-oxide nanoparticles and that the bioreduction mechanisms employed and Fe(III) reduction rates depend on the nanoparticles' aggregation state, size, shape and exposed crystal faces.

1. INTRODUCTION

Dissimilatory iron reduction (DIR) is widely observed in natural systems, and has received a great deal of attention in recent years due to the fact that as dissimilatory iron reducing bacteria (DIRB) transform Fe(III) to Fe(II) at the surface of an iron oxide particle, they also affect the mineral's surface reactivity. In doing so, the mineral's ability to adsorb or release metals, nutrients, and organic molecules is altered, which can thereby have a dramatic impact on environmental quality (Cummings et al., 1999; Zachara et al., 2001; Bonneville et al., 2004; Yan et al., 2008).

Despite all the research on DIR, there are rarely studies that systematically examine the reduction of Fe(III) nanoparticles to determine the affect that particle size and shape have on reduction rate (Yan et al., 2008). Various workers, especially in the fields of physics and chemistry, have demonstrated the novel properties that nanoparticles have, but very few studies have been conducted to systematically examine and quantify the size-dependent property changes of biogeochemical reactions in an environmentally relevant context. The small size and large surface area of mineral nanoparticles, coupled with observed changes in physical and chemical properties associated with size variability,

* Corresponding author. Fax: +1 614 292 7432.
E-mail address: lower.30@osu.edu (B.H. Lower).
[1] Present address: Energy Biosciences Institute, 271 Koshland Hall #3102, University of California at Berkeley, Berkeley, CA 94720-3102, USA.

0016-7037/$ - see front matter © 2008 Elsevier Ltd. All rights reserved.
doi:10.1016/j.gca.2008.11.031

have prompted workers to hypothesize that size-dependent-changes should also be observed in geochemical and even biogeochemical reactions (Madden and Hochella, 2005; Sparks, 2005; Madden et al., 2006).

In the present study, we examined the reduction of different size hematite (α-Fe_2O_3) nanoparticles by the DIRB *Shewanella oneidensis* MR-1, to determine how DIRB may utilize these environmentally relevant solid-phase electron acceptors. Nanoparticles used in our experiments had an average largest dimension of 11, 12, 30, 43, and 99 nm, each having one of two distinct hematite morphologies, that is, pseudo-hexagonal/irregular or rhombohedral. Hematite was selected because it is the least soluble of all iron (hydr)oxides at circumneutral pH (Baes and Mesmer, 1976; Cornell and Schwertmann, 1996) and is among the most prevalent, crystalline and thermodynamically stable iron (hydr)oxides in relatively young environments (Hansel et al., 2004) where poorly ordered phases might have been preferentially reduced by DIRB (Lovley and Phillips, 1986; Phillips et al., 1993), making hematite one of the dominant substrates for DIR and potentially a major player in controlling Fe(II)-associated geochemical cycles (Hansel et al., 2004).

Shewanella oneidensis MR-1 was selected in our study because it is a DIRB that is well known for its abilities to use a wide range of terminal electron acceptors including O_2, fumarate, trimethylamine, dimethyl sulfoxide, nitrate, nitrite, sulfite, thiosulfate, elemental sulfur, Fe(III), Mn(IV, III), Cr(VI), and U(VI) (Heidelberg et al., 2002). Because of its metabolic versatility, as well as its ability to affect the redox state of metals, *S. oneidensis* MR-1 has been studied for its potential use in the bioremediation of sites contaminated with heavy metals and metalloids (e.g. Heidelberg et al., 2002; Marshall et al., 2006).

A number of hypotheses have been proposed to explain the mechanism by which DIRB, such as *S. oneidensis* MR-1, reduce solid-phase Fe(III) under anaerobic growth conditions (Urrutia et al., 1998; Zachara et al., 1998; Lovley et al., 1999; Newman and Kolter, 2000; Beliaev et al., 2001; Lower et al., 2001, 2005, 2007; Myers and Myers, 2001; Royer et al., 2002b; Rosso et al., 2003; Reguera et al., 2005; Gorby et al., 2006; Kerisit and Rosso, 2006; Mehta et al., 2006; Shi et al., 2006; Marsili et al., 2008; von Canstein et al., 2008). Several of these studies show that direct contact between bacteria and metal oxide is required for electron transfer to occur (e.g., via outer-membrane cytochromes or nanowires), while others show that the bacteria synthesize electron shuttles (e.g., quinones, riboflavin, riboflavin-5′-phosphate, and flavin mono nucleotide) that mediate the terminal reduction of Fe(III). As the number and diversity of these hypotheses suggest, the mechanism of DIR is still not completely understood and perhaps this process may prove to be controlled through a combination of the various mechanisms described so far.

2. MATERIALS AND EXPERIMENTAL METHODS

2.1. Hematite nanoparticle synthesis

All solutions were prepared using ACS grade chemicals and were obtained from Fisher Scientific (Fair Lawn, New Jersey). Distilled, deionized water (DDW) with a resistivity of 18 MΩ cm (Millipore Corp., Milford, Massachusetts) was used for all experiments. Bottles and glassware were soaked in 0.1 N oxalic acid and rinsed with distilled water, followed by DDW.

The 11 and 12 nm nanoparticles used in this study were synthesized according to Madden and Hochella (2005) in two different batches using the forced hydrolysis of acid Fe(III) salt solutions (Schwertmann and Cornell, 2000). Briefly, 60 mL of 1.0 M ferric nitrate solution was slowly dripped into 750 mL of boiling DDW. After the ferric nitrate solution was consumed, the resulting nanoparticle solution was removed from heat and the synthesis suspension cooled overnight to room temperature. The nanoparticle solution was then dialyzed in high-grade cellulose membranes (Cellulose Sep. H1, 6000–8000 molecular weight cutoff) against DDW until the conductivity of the dialysis water reached that of pure DDW (i.e., 18 MΩ cm).

The 30 and 43 nm nanoparticles were synthesized following Madden and Hochella (2005), by bringing an Erlenmeyer flask containing 500 mL of 0.002 M HCl to a boil on a hot plate. Next, 4.04 g of $Fe(NO_3)_3{\cdot}9H_2O$ was added and the flask was vigorously shaken. Immediately, the flask was returned to the heat and held at a very mild boil for 7 days, periodically replacing evaporated water with DDW. The nanoparticle solution was removed from heat and the synthesis suspension was cooled overnight at room temperature. The nanoparticle solution was then dialyzed against DDW as described above.

The synthetic nanoparticle suspensions were then poured into HDPE bottles for storage. Part of the dialyzed suspension was subsequently transferred to 50 mL centrifuge tubes and frozen overnight at −20 °C. The frozen samples were then freeze-dried in a Labconco FreeZone 4.5 L benchtop freeze dry system (Labconco Corp. Kansas City, Missouri) prior to characterization (Xiong et al., 2006) and preserved in 50 ml sterile polypropylene centrifuge tubes.

The largest hematite nanoparticles used in this study (i.e., 99 nm) were obtained from Fisher Scientific and used as received after characterization (described below).

2.2. Hematite nanoparticle characterization

Mineralogical characterization was carried out by powder X-ray diffraction (XRD) on a Philips X'Pert MPD system with a Cu anode operating at a wavelength of 1.5406 Å ($CuK\alpha_1$) as the radiation source. Specimens were prepared by grinding the samples with a mortar and pestle to a fine powder and then placed on off-axis quartz plates (18 mm dia. × 0.5 mm DP cavity). Diffraction patterns were recorded with a proportional counter detector over a 10–60° two theta scan range at a rate of 0.025°/s. The International Center for Diffraction Data (ICDD, Newtown Square, Pennsylvania) Powder Diffraction File database on CD-ROM (ICD PDF-2, 2004 release) was used as the reference source.

Particle morphology, size distribution, and electron diffraction patterns were obtained by transmission electron microscopy (TEM). Specimens were prepared by placing a drop of nanohematite suspension onto a 200 mesh form-

var-coated copper grid (stabilized with evaporated carbon film) and allowing the DDW to evaporate. Specimens were observed in a Phillips EM 420T Scanning Transmission Electron Microscope operated in bright field mode at 100 KV. The image negatives and diffraction patterns were scanned for subsequent image analysis. Size distribution and morphology was estimated from TEM negatives on a lightbox with a 10× magnifier and measuring scale by observing approximately 100 distinguishable particles (Schwertmann, 2003) starting from the top left corner and moving systematically from top to bottom across the image.

The geometric SA calculated from TEM negatives for aggregated particles tend to overestimate the specific SA as mentioned by Madden and Hochella (2005) and hence Brunauer-Emmett-Teller (BET) surface area was used for rate calculations. Freeze dried samples were used for these measurements. Changing the degassing temperature within a certain range does not affect the SA_{BET} of these nanoparticles as previously observed by Madden and Hochella (2005); hence the degassing temperature was chosen so that it fell within this range used in our previous study. The freeze-dried powder was degassed overnight at 100 °C followed by a 6-point BET isotherm in a Quantachrome Nova 1000 N_2 Adsorption Analyzer (results shown in Table 1).

In an effort to expose roughly equivalent amounts of hematite surface area to the bacteria during dissimilatory Fe(III) reduction, the concentrations of the hematite nanoparticles in each experiment were adjusted depending upon the nanoparticle and cell size and shape. Bacterial surface area was estimated using two-dimensional measurements from TEM negatives. The surface area of a single *S. oneidensis* MR-1 bacterium was estimated to be 2.5 μm^2 based on the average diameter (0.45 μm) and length (1.8 μm) of intact bacterial cells. Using a uniform monolayer hematite nanoparticle cell coverage as a hematite concentration reference point, and taking into account the different nanohematite morphologies (i.e., the 11, 12, 99 nm nanoparticles are hexagonal platelets and the 30, 43 nm nanoparticles are rhombohedrons), for a cell density of 2×10^8 cells/mL ($OD_{600nm} = 0.24$), we assigned final hematite concentrations of 1.27, 1.97, 3.80, 3.95, and 13.5 mM for the 11, 12, 30, 43, and 99 nm nanoparticles, respectively, for each of the bioreduction assays. This rough adjustment allowed each experiment, no matter what the nanoparticle/cell spatial relationship, to have roughly similar cell to nanoparticle surface area rations. Even with this adjustment, the Fe(III) bioreduction rates were still normalized to the total hematite surface area available in each experiment (see below).

Table 1
Comparison of hematite nanoparticle surface area (SA, all measured with BET) from this study and existing literature values.

Size (nm)	SA ($m^2 g^{-1}$)	Reference
11.0	109.0	Liger et al. (1999)
11.0	96.0	This study
12.0	100.4	Liu et al. (1999)
12.0	61.9	This study
36.7	39.0	Madden and Hochella (2005)
30.0	30.9	This study
43.0	32.0	This study
88.0	9.1	Madden et al. (2006)
99.0	9.0	This study

2.3. Bacteria culture conditions

Bacteria were cultured using a continuous culture system where pH, temperature, and dissolved oxygen (DO) were controlled. A continuous culture system is a flow-through system having constant volume, differing from standard batch culture systems because fresh medium is constantly supplied to the bacterial population at a rate which limits bacterial growth, while the flow of the medium removes dead cells and waste. At equilibrium or steady state conditions, this system maintains the bacterial population at a constant density (OD_{600nm}), keeps nutrient concentrations constant, and maintains constant conditions of pH, DO, and temperature thereby better simulating bacterial growth as it occurs in natural environments (Glasauer et al., 2003; Gorby et al., 2006).

Chemicals used to prepare the growth media were purchased from Sigma Chemical Co. (St. Louis, Missouri) unless otherwise noted. *Shewanella oneidensis* MR-1 cells (wild type strain) were cultured to a steady state in a continuous flow reactor (4.0 L BIOFLO 110, New Brunswick Scientific) operating in chemostat mode with a dilution rate of 0.006 h^{-1} and a liquid volume of 3.0 L. Growth media contained the following: 18 mM sodium lactate, 3 mM PIPES buffer (1,4-piperazinediethanesulfonic acid), 28 mM ammonium chloride, 4.35 mM NaH_2PO_4, 100 mM ferric nitrilotriacetic acid, 3 mM $MgCl_2$, and 0.001 mM sodium selenate (Roden, 2003; Kukkadapu et al., 2005). Vitamins, minerals, and amino acids were provided from stock solutions as described by Kieft et al. (1999). The chemostat was supplied with excess electron acceptor ($O_2 > 2\%$ of air saturation) and agitation was maintained at 400 rpm. The pH was continuously monitored and maintained at 7.0 by using 2.0 M HCl and the temperature was held at 30 °C. O_2 served as sole terminal electron acceptor and was delivered to reactors as compressed air at a constant delivery rate of 4 L min^{-1}. Dissolved oxygen tension (DOT) was monitored using a polarographic O_2 probe and was maintained at a desired value by using a control loop and switching valves, which automatically adjusted the air-N_2 ratio of an influent gas stream (Gorby et al., 2006). The OD600nm of the culture within the chemostat was maintained at 0.35 (~4.6×10^8 cells/mL) until the cells were harvested for use in nanohematite reduction assays.

2.4. Hematite nanoparticle Fe(III) reduction assays

Bacteria were harvested from the chemostat, placed into assay tubes, and purged with N_2 gas for approximately 10 min. Reduction reactions were initiated by adding the cells to serum bottles with 1.30 mL of a previously sonicated and extensively stirred nanoparticle suspension, sodium lactate (final conc. of 10 mM) as electron donor and PIPES buffer (final conc. of 17 mM, pH 7.0) under N_2 gas, so that the final cell density was 2×10^8 cells/mL and

the final assay volume was 3 mL. Lactate was selected as the carbon source for our experiments because, among carbon sources that *S. oneidensis* MR-1 can utilize for energy, growth of these bacteria are fastest under anaerobic conditions using lactate. In addition to maintaining a pH of 7.0, we also used PIPES buffer to maintain constant hydrogen ion activity in our reduction assays. No other vitamins or trace elements were added to the assay medium. The assay medium was purged with O_2-free N_2 gas, sealed with thick butyl rubber stoppers, and then assay tubes were vertically incubated in the dark at 30 °C for time periods up to 6 h with slow gyratory shaking (i.e., 25 rpm). All experiments were run in triplicate.

At specific time-points (e.g., 2, 4 and 6 h) triplicate tubes were removed from the incubator and transferred to an anaerobic glove box (Ar:H = 95:5). The butyl rubber stoppers were removed from the assay tubes and 1.0 mL of 2 N HCl was added to the assay medium to obtain a final concentration of 0.5 N HCl (Fredrickson et al., 1998; Zachara et al., 1998). The extracts were left to equilibrate overnight in order to completely solubilize biogenic, ferrous organic complexes, as well as Fe(II) sorbed to the nanohematite and the bacteria (Fredrickson et al., 1998; Zachara et al., 1998). The next day, suspensions were filtered through a 0.2 μm polycarbonate filter to remove aggregates and 0.1 ml of the filtrate was added to 1 ml ferrozine (3-(2-pyridyl)-5,6-diphenyl-1,2,4-triazine-*p*,*P*′-disulfonic acid) (Fluka, Buchs, Switzerland) prepared (1 g/L) in 50 mM Hepes (*N*-2-hydroxyethylpiperazine-*N*′-2-ethanesulfonic acid) buffer at pH 7. Total ferrous concentration was spectrophotometrically determined by measuring the absorbance of the ferrozine-Fe(II) complex $[Fe(Fz)_3]^{2+}$ at 562 nm after 5 min of color development (Stookey, 1970; Carter, 1971; Gibbs, 1976; Thompsen and Mottola, 1984; Lovley and Phillips, 1987; Pehkonen, 1995; Zachara et al., 1998; Royer et al., 2002a; Bonneville et al., 2006). Standards of ferrous iron for the ferrozine assay were prepared with ferrous ethylene diammonium sulfate tetrahydrate (Fluka, Buchs, Switzerland) dissolved in 0.5 N HCl (Lee et al., 2007). The possible reduction by ferrozine of any Fe(III) (Pullin and Cabaniss, 2001; Pullin et al., 2004) from hematite or biogenic nanoparticles that might have passed through the filter is prevented by using Hepes buffer (pH 7). Duplicate cell-free blanks were also tested as controls at the last time-point (i.e., 6 h) to examine the extent of final abiotic Fe^{2+} in solution. The control assays contained 1.3 mL sterile anaerobic PIPES buffer (final conc. 30 mM, pH 7) in place of the bacterial cells (Zachara et al., 1998).

2.5. TEM of bacteria-nanoparticle associations

In an anaerobic chamber, whole-mount samples were prepared for TEM analysis from bacteria-nanoparticle assays just prior to terminating Fe(III) reduction assays (i.e., prior to adding 2 N HCl to the assay medium). A drop of the mineral nanoparticle-bacteria suspension was applied directly onto a 200 mesh copper grid coated with carbon-sputtered formvar support film and the grids were allowed to dry anaerobically, before being placed into an airtight mason jar in the anaerobic chamber. The samples were then removed from the anaerobic chamber and imaged using a Phillips EM 420T Scanning Transmission Electron Microscope operating in bright field mode at 100 KV and equipped with a SIA CCD camera. The samples were briefly exposed to the atmosphere before being inserted into the microscope. Images were collected and analyzed digitally with MaxImDL.

2.6. Determination of initial Fe(III) bioreduction rates

Initial rates of bacterial Fe(III) reduction (i.e., the rate at the early stages of anaerobic metabolism following the onset of anoxic conditions) were measured in this study in order to assure constant biological conditions and minimize the extent of aqueous chemical reactions that might also occur (Roden, 2004). Furthermore, a complicating factor on the long-term extent of bacterial Fe(III) reduction is the accumulation of Fe(II) on the oxide and the DIRB surfaces (Roden and Urrutia, 1999, 2002; Urrutia et al., 1999; Royer et al., 2002b), although, as explained above, the host solutions were acidified to solubilize this complexed Fe(II). Nevertheless, we felt that the most reliable assessment of the impact of particle size and shape on bacterial reduction rates could be made during the initial stages of Fe(III) reduction.

Eq. (1) shows a 1:1 molar ratio of lactate to acetate, and a 1:2 molar ration of Fe_2O_3 to Fe^{2+}. The expected half reactions and the overall reaction of lactate oxidation to acetate, coupled to the reduction of hematite is as follows (Zachara et al., 1998):

$$2Fe_2O_3(s) + CH_3CHOHCOO^-(aq) + 7H^+(aq) \rightarrow 4Fe^{2+}(aq) + CH_3COO^-(aq) + HCO_3^- + 4H_2O \quad (1)$$

The reduction reaction is:

$$Fe_2O_3(s) + 6H^+(aq) + 2e^- \rightarrow 2Fe^{2+}(aq) + 3H_2O \quad (2)$$

The oxidation reaction is:

$$CH_3CHOHCOO^-(aq) + 2H_2O \rightarrow CH_3COO^-(aq) + HCO_3^- + 5H^+(aq) + 4e^- \quad (3)$$

The reaction is far from equilibrium and hence irreversible, so the rate of production of the ferrous ion is used as an indirect measurement of the rate of reaction. As the reaction is first order with respect to $[SA_{Hematite}]$, at least in the initial stages of the reaction the rate of ferrous production should exhibit a linear trend with reaction time. Therefore, quantitative comparisons of apparent initial reduction rates (r') between particles of different sizes can be computed by fitting linear regression lines (Eq. (4)) to the total 0.5 N HCl extractable Fe(II) versus time (Rimstidt and Newcomb, 1993; Roden, 2003, 2004; Anschutz and Penn, 2005). According to the initial rate method described by Rimstidt and Newcomb (1993), the concentration of ferrous iron versus time for each bioreduction experiment was fit to the linear function:

$$[Fe^{2+}] = a_1 + b_1 t \quad (4)$$

where a_1 and b_1 give the line's y-intercept and slope, respectively, and t is time (Madden and Hochella, 2005). These

regression line fits produced coefficient of determination (r^2) values of $\geqslant 0.9$ for all experiments, very tight 95% confidence intervals and random residuals. All replicates were treated as independent data points.

The derivative of Eq. (4) equals $d[Fe^{2+}]/dt$, which also equals b_1 (i.e., the slope of the line). Thus the value of b_1 gives the initial rate of the reaction, r', at $t = 0$. The coefficient a_1 gives the initial concentration of Fe^{2+} (Madden and Hochella, 2005). The initial reaction rate r′ is the rate obtained for a particular surface area of solid used in the experiment. In order to make Fe(III) reduction rates comparable between the different nanoparticles examined here, the initial reaction rate r' for each experiment was converted to a normalized rate, r_{NOR}, which was derived by dividing r' by the total nanohematite surface area of an experiment. However, as discussed previously, for our assays the surface area of the bacterial cells were kept constant, and the surface area of the nanohematite was roughly constant. Thus, the only variables in our experiments were nanohematite total surface area, particle size and shape. Hence, surface-area-normalized Fe(III) reduction rates could be determined for each size hematite nanoparticle and compared between experiments once the reduction rate was normalized to the measured surface area of the nanohematite. All curve-fitting and statistical analysis was carried out on a Windows platform using the program JMP IN v.5.1.2 distributed by SAS Institute, Inc. (Cary, North Carolina).

3. RESULTS

3.1. Hematite nanoparticle synthesis and characterization

The X-ray diffraction powder patterns (Fig. 1) for all nanoparticles reveal that the samples are pure hematite with characteristic reflections that match the hematite reference PDF number 33-0664 from JCPDS-ICDD Powder Diffraction File (PDF-2, 2004 Release). The XRD Bragg peaks of the smaller particles exhibit peak broadening as expected for nanoparticles. The TEM micrographs (Fig. 2) and previous contact mode AFM studies (data not shown) show that the smallest nanoparticles (11 and 12 nm) are pseudo-hexagonal platelets (Fig. 2a and b), the 30 and 43 nm nanoparticles are mostly rhombic with some particles showing intergrowths (Fig. 2c and d), and the largest nanoparticles (99 nm) have pseudo-hexagonal to mostly irregular, platey morphologies (Fig. 2e). Particle size distributions were fit to normal distribution curves in JMP IN 5.1.2 and assigned mean particle sizes (mean ± SD) of 11 ± 2, 12 ± 2, 30 ± 4, 43 ± 8 nm, and 99 ± 22 nm (Fig. 3). To determine whether the mean values for the different particle sizes used in the study were statistically different from each other, a one way analysis of variance test (ANOVA), followed by an all pairs Tukey-Kramer HSD test (Sall et al., 2005) was performed. These results showed that the particle sizes used in our experiments are statically different from each other except the 11 and the 12 nm particles, which were produced in different batches using the same method and are hence denoted separately. Particle surface areas, as measured by BET surface area analysis, are shown in Table 1 for each batch of nanoparticles.

3.2. Bacterium-mineral associations as determined by TEM analysis

Fig. 4 shows the spatial relationship observed between bacterium and nanohematite in our experiments. The images presented here are considered representative of the entire sample because the same observations were seen for multiple samples. These images show the mode of adhesion, or attachment, is noticeably different between the 11, 12, 99 nm particles (Fig. 4a, b, and e, respectively) versus the 30, 43 nm nanoparticles (Fig. 4c and d, respectively). The 11, 12, and 99 nm particles are aggregated and exhibit considerably less direct contact with the bacteria than do the 30 and 43 nm particles which show little aggregation and coat the cell surfaces with comparatively uniform coverage.

Glasauer et al. (2001), in a study of bacteria–iron oxide interaction, showed that at low mineral to cell ratios, ~90% of the hematite was attached to *S. putrefaciens* CN32 cells within the first 10 min and less than 10% of the hematite was recoverable in filtrates after 24 h, irrespective of the medium pH. This observation prompted them to propose that Fe(III) reduction was due to strong binding between the mineral colloids and the cells. In this same study, TEM analysis also showed that only short exposures were needed to obtain substantial binding between the nanoparticles and cells. In our experiments the first sampling point occurred at 2 h, which is well beyond the time period required for irreversible cell-mineral adhesion as described by Glasauer et al. (2001).

3.3. Initial Fe(III) reduction rates

Considering the mM concentrations of nanohematite in each experiment in this study (see Section 2.2), one can calculate the amount of Fe(III) available for reduction considering that there are two moles of Fe(III) per mole of hematite (Eq. (1)). For the 11, 12, 30, 43, and 99 nm particles, this results in 2.54, 3.94, 7.6, 7.9, and 27 mM available Fe(III), respectively. Considering that our reduction assays contained 10 mM lactate and assuming a 1:4 stoichiometry between lactate and Fe(III) consumption (from Eq. (1)), the electron donor (i.e., lactate) was in great excess. In addition, considering the amount of Fe^{2+} produced in each experiment after 6 h (Fig. 5), and using the total Fe(III) available, only 0.06%, 0.07%, 0.01%, 0.01%, and 0.004% of the Fe(III) was reduced for the 11, 12, 30, 43, and 99 nm particles, respectively. This was also observed by Bonneville et al. (2006), in the initial stages of Fe(III) bioreduction; therefore, the amount of reduced Fe(III) is negligible when compared to the total amount of Fe(III) initially present.

We observed significant amounts of total Fe^{2+} within 2 h of initiation of Fe(III) reduction (Fig. 5). This can be seen for all particle sizes from the fact that the $t = 2$, 4, and 6 h Fe(II) levels were considerably higher than the Fe(II) concentrations of the negative controls at $t = 6$. This implies that the assays reached Fe(III) reducing conditions very quickly, and that the bacteria used up any remaining

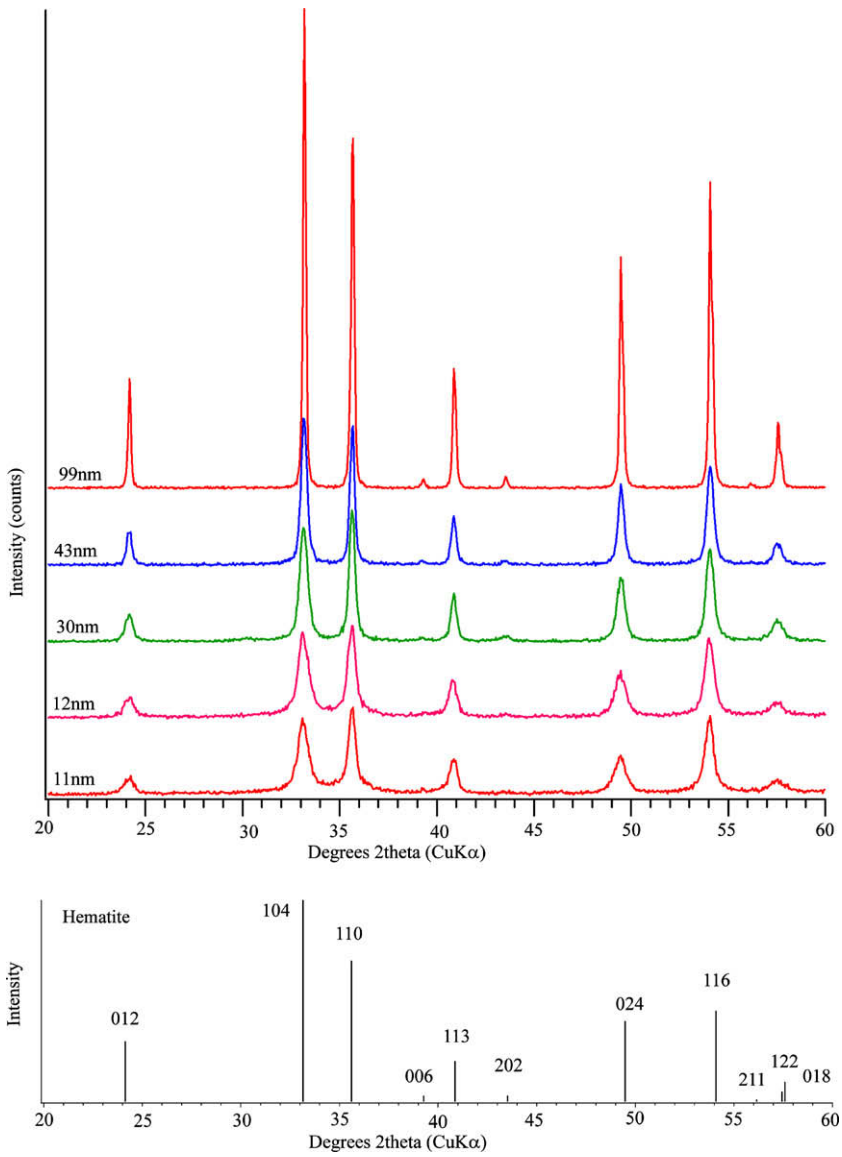

Fig. 1. XRD patterns for (a) 99 nm, (b) 43 nm, (c) 30 nm, (d) 12 nm, (e) and 11 nm (average particle size) hematite nanoparticles. The patterns were matched with the reference pattern of hematite (PDF No. 33-0664, from ICD PDF-2, 2004 release), shown at the bottom.

trace amounts of O_2 or other organic electron acceptors that might have been present in the culture media prior to reducing Fe(III).

If we compare the initial amount of Fe^{2+} at time zero to the amount of Fe^{2+} produced by the corresponding control after 6 h (Fig. 5), it is apparent that both biotic and abiotic experiments had some initial amount of Fe^{2+} prior to the start of each 6 h experiment. Among the biotic experiments, it also appears that the Fe^{2+} concentration of two of the five experimental sets (11 and 12 nm hematites) had more starting Fe^{2+} then the other three (34, 43, and 99 nm hematites). Although this excess Fe^{2+} is expected to be at least partially sorbed to the active hematite and cell membrane sites, it is interesting to note that the unnormalized reduction rates are highest for the experiments with the highest starting Fe^{2+} concentrations, and after hematite surface area normalization, these two rates bracket rates from experiments with lower starting Fe^{2+} concentrations (see Section 3.4). Therefore, we see no systematic effects of the small initial Fe^{2+} concentrations on these experiments.

The Fe(III) reduction rate data (Fig. 5) shows that total Fe^{2+} increased with time for each of the nanohematite particles tested. The percent increase of total Fe^{2+}, derived from dividing the total Fe^{2+} at $t = 6$ h by the Fe^{2+} concentration of the respective controls at $t = 6$ h, shows that the 11, 12, 30, 43, and 99 nm particles had 254%, 378%, 478%, 400%, and 434% increases in total Fe^{2+} production with respect to the controls. The linear regression fits yield coefficient of determination (r^2) values of $\geqslant 0.9$ for all experiments, very tight 95% confidence intervals and random residuals indicating that the linear regression gave very good rate estimations (Sall et al., 2005).

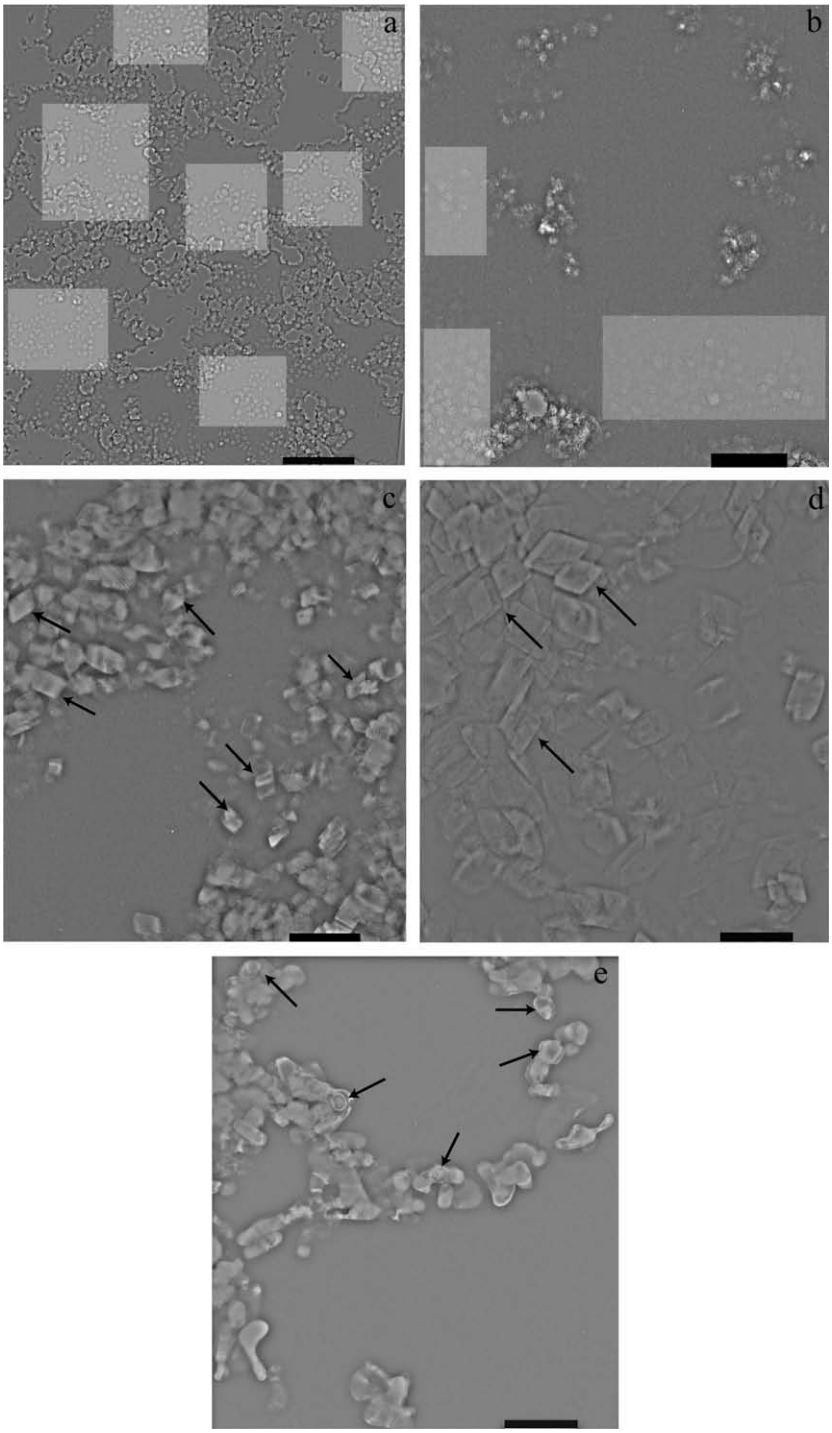

Fig. 2. TEM negatives of hematite nanoparticles with (a) 11 nm, (b) 12 nm, (c) 30 nm, (d) 43 nm, and (e) 99 nm average particle sizes. Scale bars in (a) 130 nm, (b) and (c) 80 nm, (d) 55 nm, and (e) 370 nm. The bright field TEM negatives were scanned, their tonal range was adjusted, and then they were subjected to high pass band filtering to better show the edges. Shaded boxes in (a) and (b) show areas where the pseudo-hexagonal shape can be better seen. Arrows in (c) and (d) show rhombohedral shapes and in (e) show pseudo-hexagonal to more irregular platey particles.

3.4. BET_{SA} normalized Fe(III) reduction rates

The apparent Fe(III) reduction rates, obtained from our linear regression lines (Fig. 5) were surface-area normalized (BET_{SA}) so that we could compare Fe(III) reduction rates obtained for the different nanoparticle sizes (Fig. 6). The surface-area-normalized Fe(III) reduction rates for the 11, 12, 30, and 43 nm particles group together at lower values, while the rate obtained for the 99 nm nanoparticles was considerably higher. Further-

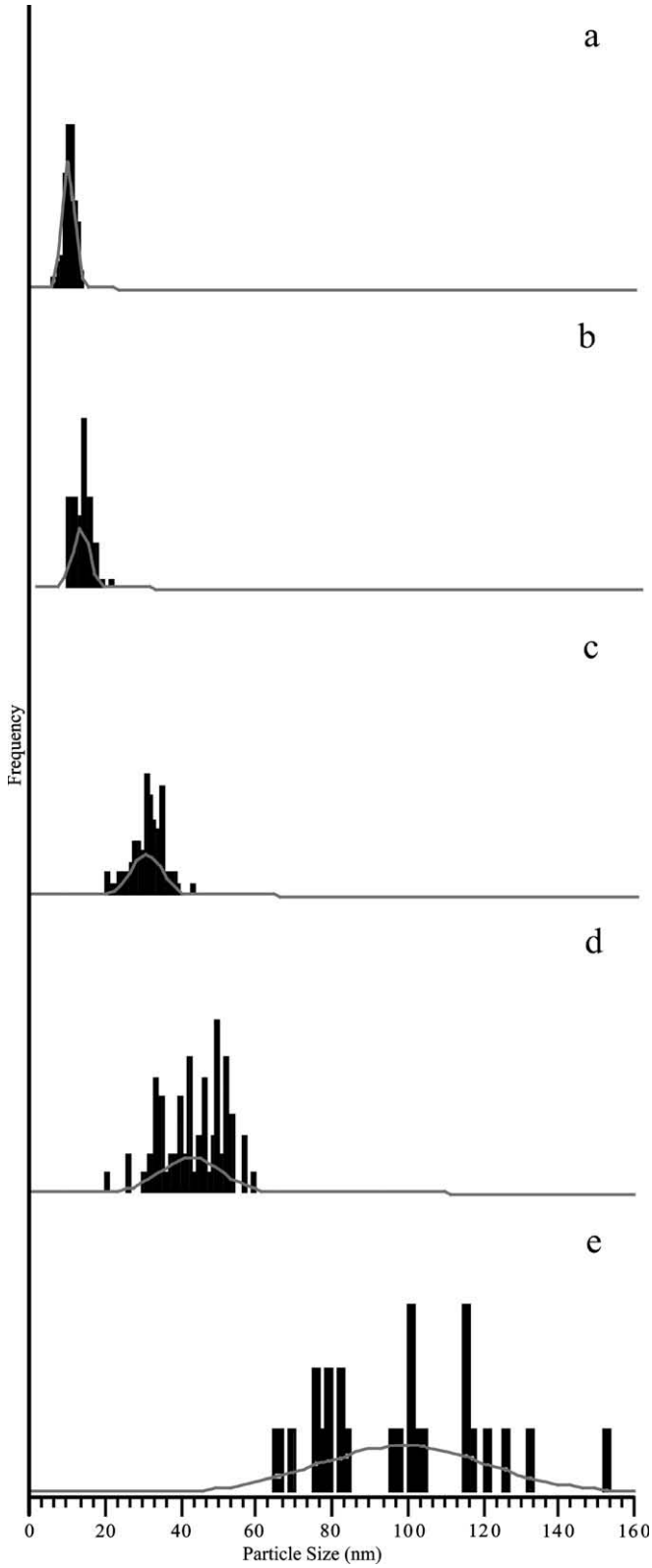

Fig. 3. Size distribution histograms generated from TEM micrographs ($n = 25$–90), and corresponding normal fit to data, compared at the same scale. Size distribution histograms give mean ± SD as reported in the text.

more, the surface-area-normalized rates for all small- to medium-sized nanoparticles (11, 12, 30, and 43 nm) fall within the same range irrespective of morphology. Our results also show that surface-area-normalized rates of

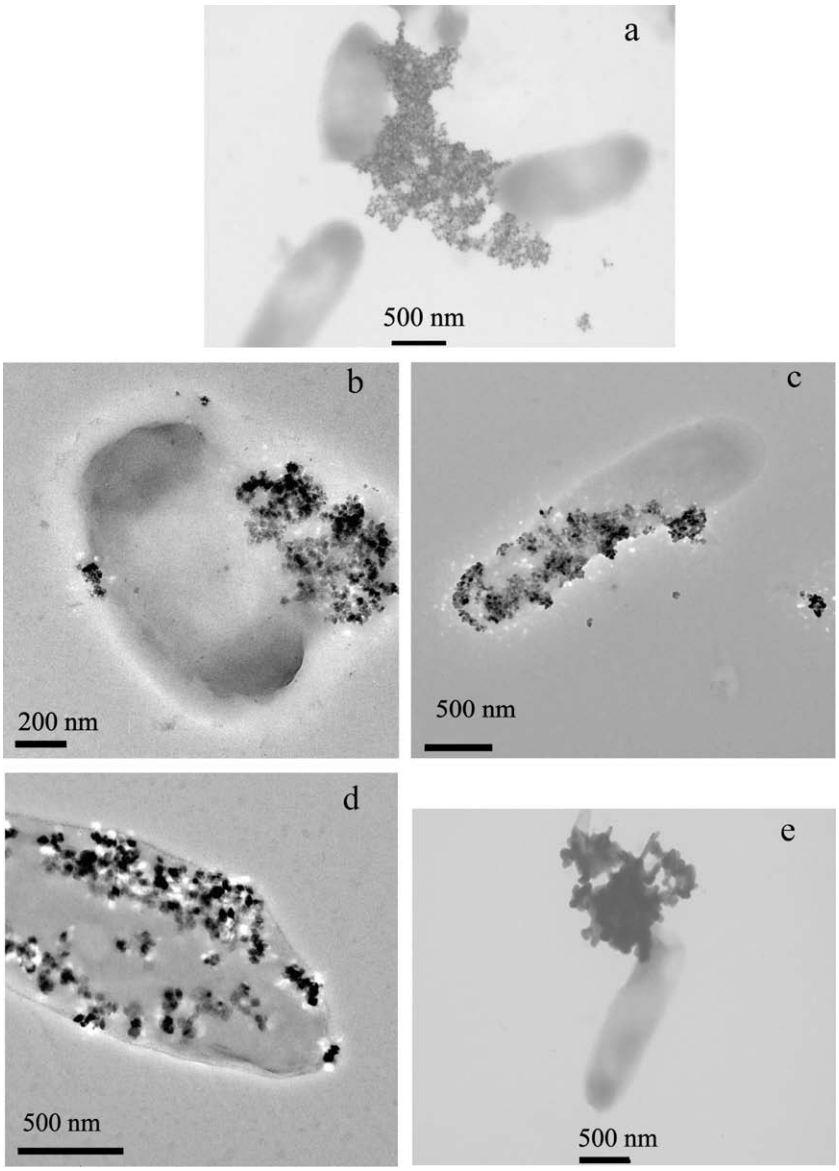

Fig. 4. TEM micrographs of whole-mount samples of *S. oneidensis* MR-1 incubated for 6 h with (a) 11 nm, (b) 12 nm, (c) 30 nm, (d) 43 nm, and (e) 99 nm hematite nanoparticles (cell density = 2×10^8 cells/mL, pH 7). Note that the 11, 12, and 99 nm particles show similar aggregation behavior, while the 30 and 43 nm particles exhibit much less aggregation and relatively uniform cell coverage.

Fe(III) reduction are fastest (by as much as 1 order of magnitude) in experiments using 99 nm hematite nanoparticles versus 11 nm nanoparticles (Fig. 6), both of which exhibit similar modes of cellular attachment. The surface-area-normalized Fe(III) reduction rates observed for the 12 nm particles are greater than the 11 nm particles and fall between the values obtained for the 11 nm and the 99 nm nanoparticles. Although the 30 and 43 nm nanoparticles have different morphology and modes of cell attachment than do the 11 and 12 nm nanoparticles (Fig. 4), the rates of Fe(III) reduction for these nanoparticles occur within the same range as the 11 and the 12 nm particles (Fig. 6). The rates are lower compared to previous studies and the differences might be due to various reasons as discussed in Section 4.

4. DISCUSSION

Previous work suggests that *Shewanella* changes its mode of electron transfer from a direct to indirect mechanism depending upon nutrients contained within the growth medium (Lies et al., 2005). Our study suggests a similar explanation framework in that nanohematite morphology, particle size, and/or degree of aggregation seem to influence the mechanism that *S. oneidensis* MR-1 utilizes to access and reduce Fe(III) sites on nanohematite surfaces.

Comparison of the surface-area-normalized Fe(III) reduction rates (Fig. 6) shows that nanoparticles of different sizes and shapes but exhibiting similar modes of cell attachment (i.e., the 11, 12, and 99 nm particles; Fig. 4a, b, and e) are reduced at rates different by as much as one order of

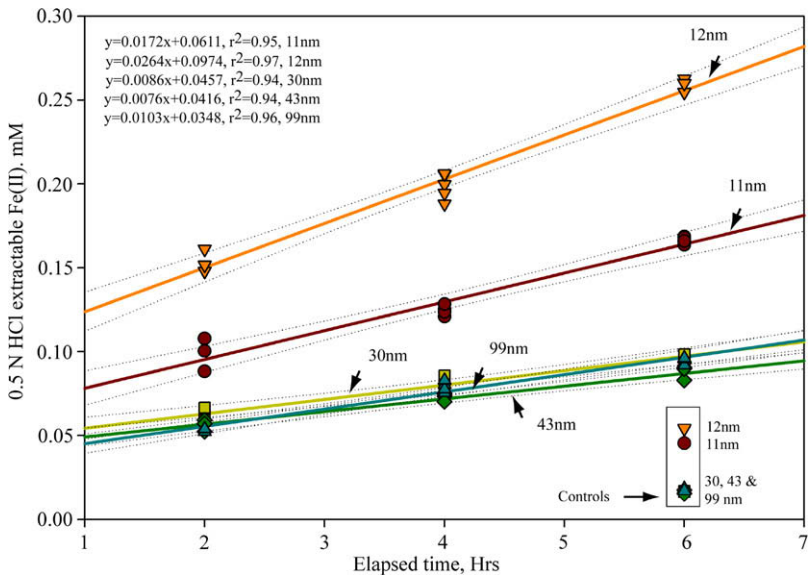

Fig. 5. Comparison of Fe(III) reduction rates for different sized nanoparticles using the method of initial rates. Shown is the 0.5 N HCl extractable $[Fe^{2+}]_{total}$ in mM versus elapsed time (given in hours), showing first order rates of Fe(II) production from 2 to 6 h. All experiments contained 17 mM PIPES (pH 7.0) and 10 mM lactate. The controls contained 30 mM PIPES (pH 7.0) instead of bacterial cells and 10 mM lactate. The solid lines represent linear regression analysis of the data and the dashed lines represent the 95% confidence intervals. Equations and coeffecients of regression (r^2) values determined from linear regression analysis are given for each size fraction of hematite nanoparticle assayed. Each time-point has $n = 3$–6 measurements for each particle size. The cell-free controls were measured in duplicate and are shown at the right hand bottom corner.

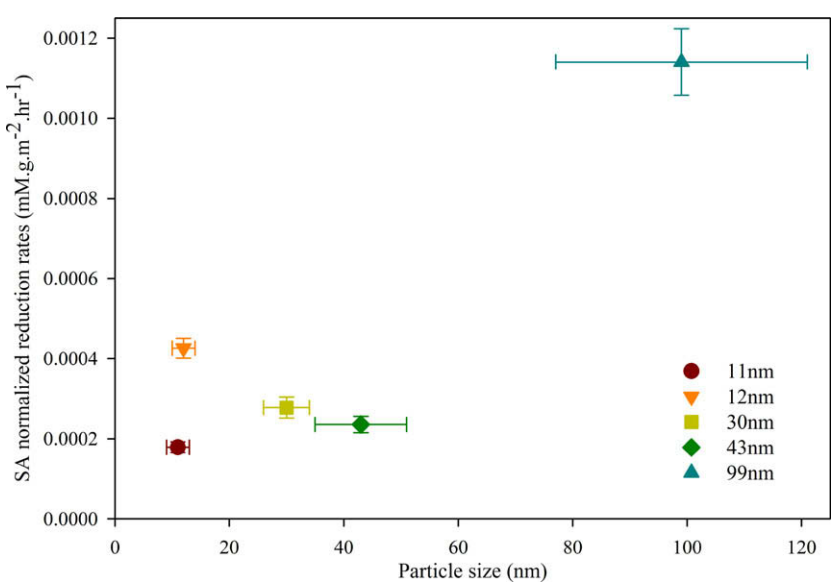

Fig. 6. Initial Fe(III) reduction rates given by linear least squares regression analysis of total Fe(II) versus time. SA_{BET} normalized Fe(III) reduction rates (mM g/m^2 Hr) is plotted versus time (h). Data presented is for triplicate 3 mL cultures, for each nanoparticle size, at each time-point. Surface-area-normalized Fe(III) reduction rates were derived by dividing the initial Fe(III) reduction rates by the corresponding SA_{BET}. X-error bars = 1 standard deviation of the particle size analysis, Y-error bars = SA normalized std. error of the slopes of linear regression fit to total Fe(II) versus time data. Error bars not visible are smaller than symbols.

magnitude. For these nanohematite particles we observed a general trend that surface-area-normalized Fe(III) reduction rates increased with increasing particle size (i.e., the reduction rates for the 99 nm nanohematite >> 12 nm nanohematite > 11 nm nanohematite). Conversely, comparison of the surface-area-normalized Fe(III) reduction rates for nanoparticles exhibiting vastly different modes of cellular attachment (i.e., the 11 and 12 nm particles versus the 30 and 43 nm particles; Fig. 4) shows that the reduction rates of these nanoparticles are relatively similar. These re-

sults, coupled with the percent of Fe^{3+} reduced, the percent increase in Fe^{2+}, and the TEM micrographs showing that the 11, 12, and 99 nm hematite particles (Fig. 4a, b, and e) attach to the cells differently than the 30 and 43 nm particles (Fig. 4c and d), suggest the possibility that *S. oneidensis* MR-1 uses more than one mechanism to respire Fe(III)-oxide nanoparticles.

Previous studies have shown that indirect electron shuttling mechanisms of DIR are a more efficient means for DIRB to reduce crystalline Fe(III) (e.g., hematite) compared to mechanisms that employ direct contact between the bacteria and Fe(III)-oxide (Lovley et al., 1998; Zachara et al., 1998; Royer et al., 2002b). These studies show that electron shuttles may accelerate bacterial reduction of crystalline Fe(III)-oxides because they permit transfer of electrons to iron oxides that are not readily reduced due to, for example, aggregated states where small pore spaces are not accessible to DIRB. Our study suggests that *S. oneidensis* MR-1 may be utilizing, at least in part, a direct contact mechanism to reduce the dispersed 30 and 43 nm Fe_2O_3 nanoparticles, and primarily an indirect shuttling mechanism of bacteria-to-Fe_2O_3 electron transfer to respire the aggregated 11, 12, and 99 nm particles.

4.1. Factors influencing the bioreduction of hematite nanoparticles

In the experiments presented here, culture conditions, bacterial cell density, ionic strength, and basic mineralogy were kept constant for all nanoparticle sizes assayed, and the nanohematite surface areas available were similar for each experiment. However, differences in nanoparticle morphology, size, solubility, and aggregation state, and Fe(II) adsorption to both mineral and cell surfaces, could all potentially effect Fe(III) reduction rates (Roden and Zachara, 1996; Zachara et al., 1998; Glasauer et al., 2001; Neal et al., 2003, 2005; Roden, 2003; Rosso et al., 2003; Bonneville et al., 2004; Yan et al., 2008).

The pzc for hematite nanoparticles suggest that they may be unstable against aggregation at pH ~ 7 (i.e., pH of the growth medium used in our experiments) and the resulting aggregates may possess complex interior porosity (Gilbert and Banfield, 2005). For example, at pH ~ 7, the 11 nm nanohematite self-associates to form a broad distribution of particle sizes ranging from a few nanometers to large aggregates with an apparent size of about 400 nm (Xiong et al., 2006). It is also known that solute ions can adsorb to nanohematite thereby mitigating surface charges and enhancing nanoparticle aggregation (Schwertmann and Cornell, 2000). This will result in decreased nanohematite surface area, and thus decrease the amount of surface-exposed Fe(III) accessible to the bacteria for direct electron transfer, which should likewise result in diminished initial rates of Fe(III) reduction (Roden, 2003) if the mechanism of terminal Fe(III) reduction occurred exclusively via direct contact between bacterium and Fe(III)-oxide surface.

All nanohematite suspensions were prepared from 10× stock solutions which were ultrasonicated for 30 min and then stirred with a Teflon stir bar on a magnetic stirrer, for at least 1 h prior to culture inoculation. The reduction assays were carried out at pH 7, and no attempt was made to disaggregate the particles by adjusting the pH to 5, because this process is reported to reduce *S. oneidensis* MR-1 viability (Claessens et al., 2004, 2006; Bonneville et al., 2006). The differences in the aggregation behavior between the 11, 12, and 99 nm versus the 30 and 43 nm particles could be explained by (a) the size and shape dependence of metal oxide nanoparticle interaction energies (Kallay and Zalac, 2002; Gilbert et al., 2007) and (b) the fact that the largest particles (99 nm) were obtained in a dried form, and hence were impossible to completely resuspend even after being subjected to mechanical agitation and intense sonication. Although much remains to be understood about metal oxide nanoparticle aggregation, apparently the overall size and faces exposed on the 30 and 43 nm particles provide significant overall repulsive Coulombic forces between particles, greatly reducing aggregate stability at least under the solution and pH conditions of our experiments. However, electrostatic attraction to the cell membrane surfaces assures rapid attachment to the bacteria, as observed. Despite obvious dispersion instability (or aggregate stability) for the 11 and 12 nm particles throughout our experiments, attractive forces still exist between the nanoclusters and cells and nanocluster/cell association is common. The 99 nm commercial nanoparticles also form aggregates likely due to a combination of commercial synthesis and sample handling protocols (these methods are proprietary, but we do know that this nanohematite is synthesized through a precipitation process, and then the material is thoroughly dried). Like the nanoclusters of the 11 and 12 nm particles, the 99 nm clusters are still attracted, and remain attached, to the bacterial cells. The higher reduction rate of the irregular and strongly aggregated 99 nm particles certainly warrants further investigation, and could be related to the production method. However, it should also be noted that recent work by Cwiertny et al. (2008) indicates unreliability in using BET of dry powders as a realistic estimate of the amount of surface area accessible for sorption and reaction in wet nanoparticle suspensions, at least for the large dense nanogoethite aggregates used in their study.

Conductive nanowires containing outer-membrane cytochromes (Gorby et al., 2006) may also be used as a mechanism of electron transfer by *S. oneidensis* MR-1; however, at least in these experiments, evidence for nanowires were not seen in any of our TEM images, so we do not believe that nanowires were involved in DIR here.

Wang et al. (2003) show that semiconductor aggregates (e.g., hematite) are very efficient at consuming and transporting electrons within the aggregate. Kerisit and Rosso (2006) recently calculated fast electron transfer rates (i.e., picosecond to nanosecond) within an hematite lattice because of the close proximity of electron transfer centers in the hematite solid-phase. As described above, our results show that although aggregation can have an effect on the mode of bacterial-nanoparticle attachment, it does not negatively impact the rate of dissimilatory Fe(III) reduction. We have suggested that this is because the bacteria are utilizing indirect shuttling mechanisms to reduce Fe(III) sites contained within the nanohematite aggregates. However, reactive efficiency could also be promoted by electron trans-

port within and between particles in the aggregates; for example, transferring electrons within the hematite structure and away from the bacterium–hematite interface may be important in regenerating Fe(III) sites at the interface which could be reduced repeatedly.

4.2. The role of nanoparticle electronic structure on Fe(III) reduction

The fact that we observed one order of magnitude difference in Fe(III) reduction rates between the largest (99 nm) and smallest nanoparticles (11 nm) was rather curious because these two nanoparticles show similar modes of attachment to the bacterial cells (Fig. 6a and e). One explanation may come from recent studies that show the reactivity of hematite nanoparticles change as a function of nanoparticle size (Madden and Hochella, 2005). Such changes can be attributed to differences in the surface bonding environments of the different sized nanohematite (Madden and Hochella, 2005), thermodynamic stability effects (Navrotsky, 2001; Waychunas et al., 2005), or differences in the internal and surface atomic structures of the hematite nanoparticles (Waychunas et al., 2005). Previous studies have also demonstrated that redox processes can be affected by modification of the absolute valence and conduction-band energy levels of semiconductors (e.g., hematite) resulting from a size-dependent variation in bandgap energy (Gilbert and Banfield, 2005; Madden and Hochella, 2005; Madden et al., 2006; Yang and Jiang, 2006). This can have an affect on a mineral's reactivity, especially when a nanoparticle accepts or donates electrons, or acts as redox-active species in solution. However, this possibility seems unlikely here, in light of recent X-ray spectroscopy on hematite nanoparticles (Gilbert, 2007) which showed no band gap variations down to particles sizes of 7 nm.

4.3. Effect of increasing solubility with decreasing nanoparticle size on Fe(III) reduction

The thermodynamic stability of different phases of iron (oxy)hydroxides change with their particle size and crystal structure (Hansel et al., 2004; Navrotsky et al., 2008). In general, bulk mineral solubility is predicted to increase as particle size decreases (Stumm and Morgan, 1996), assuming that the interfacial energy is not particle size-dependent, an assumption that has been questioned recently by Zhang et al. (1999). Still, because the surface free energies of iron oxides are relatively high and smaller particles sizes have higher surface areas, smaller hematite nanoparticles are predicted to have increased solubility (Schwertmann and Cornell, 2000). However, the surface-area-normalized Fe(III) reduction rates (Fig. 6) show that smaller hematite nanoparticles exhibit lower rates of Fe(III) reduction, and therefore lower dissolution rates, compared to the larger nanoparticles used in this study. While this observation is contrary to what may be expected in terms of dissolution, it is consistent with recent reports that show brushite ($CaHPO_4{\cdot}2H_2O$) particles smaller than a critical size (defect spacing) actually show inhibited mineral dissolution (Tang et al., 2004). The exact effect that nanoparticle solubility and size has on nanohematite reduction by *S. oneidensis* MR-1 is not discernable from data presented here, but does warrant future exploration.

4.4. Effect of Fe(II) surface passivation and biomineralization on Fe(III) reduction

Another potential controlling factor of bacterial Fe(III) reduction is the phenomena of mineral- or cell surface passivation by adsorbed Fe(II). DIRB produce biogenic Fe^{2+} which can exist as Fe^{2+} (aq), mineral-sorbed Fe(II), or as biosorbed Fe(II). Soluble Fe^{2+} is strongly adsorbed onto hematite at circumneutral pH (Fredrickson et al., 1998). A recent study (Hansel et al., 2004) showed that for long-term (16 days) reduction of hematite particles by *S. putrefaciens* CN32, Fe(III) reduction could be divided into two stages: an early stage defined by rapid Fe(III) reduction that was controlled by the initial surface disorder (high energy sites) of hematite particles themselves; and a later stage defined by a sustained slower Fe(III) reduction of lower energy sites. Hansel et al. (2004) suggest that the surface reactivity and oxidizing capacity of the nanohematite decreased over the long-term, as a result of higher energy sites being gradually replaced by localized low energy magnetite-like surface sites or transduction within the bulk phase by delocalized electrons. Therefore, higher initial rates of Fe(III) reduction would produce greater amounts of Fe(II) that would accumulate on the nanohematite surface (Hansel et al., 2004), thereby passivating the surface of the nanoparticles making reactive sites less available to sustain Fe(III) reduction.

DIRB also mediate the formation of Fe-mineral phases from soluble Fe^{2+} produced as a result of direct or indirect electron transfer processes (Zachara et al., 2002; Glasauer et al., 2003). These biomineral by-products strongly influence the thermodynamics and kinetics of dissimilatory Fe(III) reduction by either enhancing Fe(III) bioreduction as a result of expending and thus removing dissimilatory by-products like Fe^{2+}, or hindering Fe(III) bioreduction by passivating the Fe(III)-oxide surface or DIRB surface with biomineral product (Liu et al., 2001a,b; Zachara et al., 2002).

The assay medium used here was composed of lactate, PIPES buffer, cells, and mineral suspension, in order to keep the ionic strength of the solution to a minimum, maintain a constant pH, and thus limit secondary mineral formation. We also terminated the experiments relatively early (i.e., 6 h) compared to the longer time periods required for Fe(II) mass transfer or biomineralization (Zachara et al., 1998; Glasauer et al., 2003; Royer et al., 2004). Furthermore, the bioreduction-assay medium contained no soluble PO_4^{-3} so that we would not promote phosphate-induced biomineralization. In our experiments, we did not observe divergent-needle-like crystals (Glasauer et al., 2003) nor did we observe prismatic crystals (Zachara et al., 2002), which are characteristics of vivianite [$Fe_3(PO_4)_2{\cdot}8H_2O$]. Green rust, a metastable precursor of magnetite, and vivianite can also form in the presence of PO_4^{-3} and organic buffers (Zachara et al., 2002); however, no instances of electron dense hexagonal crystals of green rust

were found for any of the bioreduced cell-mineral associations. Therefore, because we used well defined medium in our experiments, relatively short assay times, and because of the fact that no biomineral products were observed for any of nanohematite-bacteria associations, we do not believe that biomineralization processes had any affects on DIR in our experiments.

5. CONCLUSIONS AND FURTHER CONSIDERATIONS

To our knowledge, this is one of the first studies to systematically examine the effect that Fe(III)-oxide nanoparticle size has on DIR. Our results suggest that *S. oneidensis* MR-1 utilizes different mechanisms of electron transfer to reduce Fe(III) sites on mineral nanoparticles, and that the mechanism it employs depends, at least in part, on the aggregation of the Fe(III)-nanoparticles. Furthermore, the overall rate of Fe(III) reduction depends on the size and shape of the nanoparticles. Additional experiments are needed to determine whether the same types of trends in surface-area-normalized metal reduction rates hold for other iron and manganese oxide nanoparticles. Experiments are also needed to determine whether *S. oneidensis* MR-1 activates different components of its electron transfer system (e.g., synthesizes particular proteins) as it respires anaerobically using different iron and manganese oxide (e.g., hematite, goethite, manganite) nanoparticles as terminal electron acceptors.

ACKNOWLEDGMENTS

A portion of this research was performed as part of an EMSL Scientific Grand Challenge project at the W.R. Wiley Environmental Molecular Sciences Laboratory, a national scientific user facility sponsored by the US Department of Energy's (DOE) Office of Biological and Environmental Research (OBER) and located at Pacific Northwest National Laboratory (PNNL). PNNL is operated for the DOE by Battelle Memorial Institute under Contract DE-AC05-76RL01830. M.F.H. and B.H.L. acknowledge the DOE Office of Basic Energy Sciences (OBES) Geosciences Research Program. M.F.H. recognizes DOE-OBES Grant DE-FG02-06ER15786. S.B. gratefully acknowledges Stephen McCartney (VT) and Alice Dohnalkova (PNNL) for help with TEM and support from the Mineralogical Society of America and the Virginia Tech Graduate Students Association. We thank J. Fredrickson, D. Rimstidt, and J. Zachara for their insightful comments regarding the scope and focus of this paper. The comments and suggestions of Johnson R. Hass, Benjamin Gilbert and two anonymous reviewers greatly helped improve the original manuscript and are gratefully acknowledged.

REFERENCES

Anschutz A. J. and Penn R. L. (2005) Reduction of crystalline iron(III) oxyhydroxides using hydroquinone: influence of phase and particle size. *Geochemical Transactions* **6**, 60–66.

Baes C. F. and Mesmer R. E. (1976) *The Hydrolysis of Cations*. Wiley, New York.

Beliaev A. S., Saffarini D. A., Mclaughlin J. L. and Hunnicutt D. (2001) MtrC, an outer membrane decahaem*c* cytochrome required for metal reduction in *Shewanella putrefaciens* MR-1. *Molecular Microbiology* **39**, 722–730.

Bonneville S., Behrends T., Van Cappellen P., Hyacinthe C. and Roling W. F. M. (2006) Reduction of Fe(III) colloids by *Shewanella putrefaciens*: a kinetic model. *Geochimica et Cosmochimica Acta* **70**, 5842–5854.

Bonneville S., Van Cappellen P. and Behrends T. (2004) Microbial reduction of iron(III) oxyhydroxides: effects of mineral solubility and availability. *Chemical Geology* **212**, 255–268.

Carter P. (1971) Spectrophotometric determination of serum iron at the submicrogram level with a new reagent (ferrozine). *Analytical Biochemistry* **40**, 450–458.

Claessens J., Behrends T. and Van Cappellen P. (2004) What do acid-base titrations of live bacteria tell us? A preliminary assessment. *Aquatic Sciences* **66**, 19–26.

Claessens J., Van Lith Y., Laverman A. M. and Van Cappellen P. (2006) Acid-base activity of live bacteria: implications for quantifying cell wall charge. *Geochimica et Cosmochimica Acta* **70**, 267–276.

Cornell R. M. and Schwertmann U. (1996) *The Iron Oxides: Structure, Properties, Reactions, Occurrence and Uses*. VCH.

Cummings D. E., Caccavo F., Fendorf S. and Rosenzweig R. F. (1999) Arsenic mobilization by the dissimilatory Fe(III)-reducing bacterium *Shewanella alga* BrY. *Environmental Science & Technology* **33**, 723–729.

Cwiertny D. M., Handler R. M., Schaefer M. V., Grassian V. H. and Scherer M. M. (2008) Interpreting nanoscale size-effects in aggregated Fe-oxide suspensions: reaction of Fe(II) with goethite. *Geochimica et Cosmochimica Acta* **72**, 1365–1380.

Fredrickson J. K., Zachara J. M., Kennedy D. W., Dong H. L., Onstott T. C., Hinman N. W. and Li S. M. (1998) Biogenic iron mineralization accompanying the dissimilatory reduction of hydrous ferric oxide by a groundwater bacterium. *Geochimica et Cosmochimica Acta* **62**, 3239–3257.

Gibbs C. R. (1976) Characterization and application of Ferrozine iron reagent as a Ferrous iron indicator. *Analytical Chemistry* **48**, 1197–1201.

Gilbert B. (2007) Surface and electronic structure effects on interfacial charge transfer at iron oxide nanoparticle surfaces. *Geochimica et Cosmochimica Acta* **71**, A323.

Gilbert B. and Banfield J. F. (2005) Molecular-scale processes involving nanoparticulate minerals in biogeochemical systems. *Molecular Geomicrobiology* **59**, 109–155.

Gilbert B., Lu G. P. and Kim C. S. (2007) Stable cluster formation in aqueous suspensions of iron oxyhydroxide nanoparticles. *Journal of Colloid and Interface Science* **313**, 152–159.

Glasauer S., Langley S. and Beveridge T. J. (2001) Sorption of Fe (hydr)oxides to the surface of *Shewanella putrefaciens*: cell-bound fine-grained minerals are not always formed de novo. *Applied and Environmental Microbiology* **67**, 5544–5550.

Glasauer S., Weidler P. G., Langley S. and Beveridge T. J. (2003) Controls on Fe reduction and mineral formation by a subsurface bacterium. *Geochimica et Cosmochimica Acta* **67**, 1277–1288.

Gorby Y. A., Yanina S., Mclean J. S., Rosso K. M., Moyles D., Dohnalkova A., Beveridge T. J., Chang I. S., Kim B. H., Kim K. S., Culley D. E., Reed S. B., Romine M. F., Saffarini D. A., Hill E. A., Shi L., Elias D. A., Kennedy D. W., Pinchuk G., Watanabe K., Ishii S., Logan B., Nealson K. H. and Fredrickson J. K. (2006) Electrically conductive bacterial nanowires produced by *Shewanella oneidensis* strain MR-1 and other microorganisms. *Proceedings of the National Academy of Sciences* **103**, 11358–11363.

Hansel C. M., Benner S. G., Nico P. and Fendorf S. (2004) Structural constraints of ferric (hydr)oxides on dissimilatory iron reduction and the fate of Fe(II). *Geochimica et Cosmochimica Acta* **68**, 3217–3229.

Heidelberg J. F., Paulsen I. T., Nelson K. E., Gaidos E. J., Nelson W. C., Read T. D., Eisen J. A., Seshadri R., Ward N., Methe B., Clayton R. A., Meyer T., Tsapin A., Scott J., Beanan M., Brinkac L., Daugherty S., Deboy R. T., Dodson R. J., Durkin A. S., Haft D. H., Kolonay J. F., Madupu R., Peterson J. D., Umayam L. A., White O., Wolf A. M., Vamathevan J., Weidman J., Impraim M., Lee K., Berry K., Lee C., Mueller J., Khouri H., Gill J., Utterback T. R., Mcdonald L. A., Feldblyum T. V., Smith H. O., Venter J. C., Nealson K. H. and Fraser C. M. (2002) Genome sequence of the dissimilatory metal ion-reducing bacterium *Shewanella oneidensis*. *Nature Biotechnology* **20**, 1118–1123.

Kallay N. and Zalac S. (2002) Stability of nanodispersions: a model for kinetics of aggregation of nanoparticles. *Journal of Colloid and Interface Science* **253**, 70–76.

Kerisit S. and Rosso K. M. (2006) Computer simulation of electron transfer at hematite surfaces. *Geochimica et Cosmochimica Acta* **70**, 1888–1903.

Kieft T. L., Fredrickson J. K., Onstott T. C., Gorby Y. A., Kostandarithes H. M., Bailey T. J., Kennedy D. W., Li S. W., Plymale A. E., Spadoni C. M. and Gray M. S. (1999) Dissimilatory reduction of Fe(III) and other electron acceptors by a *Thermus* isolate. *Applied and Environmental Microbiology* **65**, 1214–1221.

Kukkadapu R. K., Zachara J. M., Fredrickson J. K., Kennedy D. W., Dohnalkova A. C. and Mccready D. E. (2005) Ferrous hydroxy carbonate is a stable transformation product of biogenic magnetite. *American Mineralogist* **90**, 510–515.

Lee J.-H., Roh Y., Kim K.-W. and Hur H.-G. (2007) Organic acid-dependent iron mineral formation by a newly isolated iron-reducing bacterium, Shewanella sp. HN-41. *Geomicrobiology Journal* **24**, 31–41.

Lies D. P., Hernandez M. E., Kappler A., Mielke R. E., Gralnick J. A. and Newman D. K. (2005) *Shewanella oneidensis* MR-1 uses overlapping pathways for iron reduction at a distance and by direct contact under conditions relevant for biofilms. *Applied and Environmental Microbiology* **71**, 4414–4426.

Liger E., Charlet L. and Van Cappellen P. (1999) Surface catalysis of uranium(VI) reduction by iron(II). *Geochimica et Cosmochimica Acta* **63**, 2939–2955.

Liu C. G., Zachara J. M., Gorby Y. A., Szecsody J. E. and Brown C. F. (2001a) Microbial reduction of Fe(III) and sorption/precipitation of Fe(II) on *Shewanella putrefaciens* strain CN32. *Environmental Science & Technology* **35**, 1385–1393.

Liu C. X., Kota S., Zachara J. M., Fredrickson J. K. and Brinkman C. K. (2001b) Kinetic analysis of the bacterial reduction of goethite. *Environmental Science & Technology* **35**, 2482–2490.

Liu X. Y., Ding J. and Wang J. (1999) An alpha-Fe_2O_3 powder of nanosized particles via precursor dispersion. *Journal of Materials Research* **14**, 3355–3362.

Lovley D. R., Fraga J. L., Blunt-Harris E. L., Hayes L. A., Phillips E. J. P. and Coates J. D. (1998) Humic substances as a mediator for microbially catalyzed metal reduction. *Acta Hydrochimica Et Hydrobiologica* **26**, 152–157.

Lovley D. R., Fraga J. L., Coates J. D. and Blunt-Harris E. L. (1999) Humics as an electron donor for anaerobic respiration. *Environmental Microbiology* **1**, 89–98.

Lovley D. R. and Phillips E. J. P. (1986) Availability of ferric iron for microbial reduction in bottom sediments of the fresh-water tidal Potomac river. *Applied and Environmental Microbiology* **52**, 751–757.

Lovley D. R. and Phillips E. J. P. (1987) Rapid assay for microbially reducible ferric iron in aquatic sediments. *Applied and Environmental Microbiology* **53**, 1536–1540.

Lower B. H., Hochella M. F. and Lower S. K. (2005) Putative mineral-specific proteins synthesized by a metal reducing bacterium. *American Journal of Science* **305**, 687–710.

Lower B. H., Shi L., Yongsunthon R., Droubay T. C., Mccready D. E. and Lower S. K. (2007) Specific bonds between an iron oxide surface and outer membrane cytochromes MtrC and OmcA from *Shewanella oneidensis* MR-1. *Journal of Bacteriology* **189**, 4944–4952.

Lower S. K., Hochella M. F. and Beveridge T. J. (2001) Bacterial recognition of mineral surfaces: nanoscale interactions between *Shewanella* and alpha-FeOOH. *Science* **292**, 1360–1363.

Madden A. S. and Hochella M. F. (2005) A test of geochemical reactivity as a function of mineral size: manganese oxidation promoted by hematite nanoparticles. *Geochimica et Cosmochimica Acta* **69**, 389–398.

Madden A. S., Hochella M. F. and Luxton T. P. (2006) Insights for size-dependent reactivity of hematite nanomineral surfaces through Cu^{2+} sorption. *Geochimica et Cosmochimica Acta* **70**, 4095–4104.

Marshall M. J., Beliaev A. S., Dohnalkova A. C., Kennedy D. W., Shi L., Wang Z. M., Boyanov M. I., Lai B., Kemner K. M., Mclean J. S., Reed S. B., Culley D. E., Bailey V. L., Simonson C. J., Saffarini D. A., Romine M. F., Zachara J. M. and Fredrickson J. K. (2006) C-type cytochrome-dependent formation of U(IV) nanoparticles by *Shewanella oneidensis*. *Plos Biology* **4**, 1324–1333.

Marsili E., Baron D. B., Shikhare I. D., Coursolle D., Gralnick J. A. and Bond D. R. (2008) Shewanella Secretes flavins that mediate extracellular electron transfer. *Proceedings of the National Academy of Sciences* **105**, 3968–3973.

Mehta T., Childers S. E., Glaven R., Lovley D. R. and Mester T. (2006) A putative multicopper protein secreted by an atypical type II secretion system involved in the reduction of insoluble electron acceptors in *Geobacter sulfurreducens*. *Microbiology* **152**, 2257–2264.

Myers J. M. and Myers C. R. (2001) Role for outer membrane cytochromes OmcA and OmcB of *Shewanella putrefaciens* MR-1 in reduction of manganese dioxide. *Applied and Environmental Microbiology* **67**, 260–269.

Navrotsky A. (2001) Thermochemistry of nanomaterials. *Nanoparticles and the Environment* **44**, 73–103.

Navrotsky A., Mazeina L. and Majzlan J. (2008) Size-driven structural and thermodynamic complexity in iron oxides. *Science* **319**, 1635–1638.

Neal A. L., Bank T. L., Hochella M. F. and Rosso K. M. (2005) Cell adhesion of *Shewanella oneidensis* to iron oxide minerals: effect of different single crystal faces. *Geochemical Transactions* **6**, 77–84.

Neal A. L., Rosso K. M., Geesey G. G., Gorby Y. A. and Little B. J. (2003) Surface structure effects on direct reduction of iron oxides by *Shewanella oneidensis*. *Geochimica et Cosmochimica Acta* **67**, 4489–4503.

Newman D. K. and Kolter R. (2000) A role for excreted quinones in extracellular electron transfer. *Nature* **405**, 94–97.

Pehkonen S. (1995) Determination of the oxidation states of iron in natural waters. A review. *Analyst* **120**, 2655–2663.

Phillips E. J. P., Lovley D. R. and Roden E. E. (1993) Composition of non-microbially reducible Fe(III) in aquatic sediments. *Applied and Environmental Microbiology* **59**, 2727–2729.

Pullin M. J. and Cabaniss S. E. (2001) Colorimetric flow-injection analysis of dissolved iron in high DOC waters. *Water Research* **35**, 363–372.

Pullin M. J., Progess C. A. and Maurice P. A. (2004) Effects of photoirradiation on the adsorption of dissolved organic matter to goethite. *Geochimica et Cosmochimica Acta* **68**, 3643–3656.

Reguera G., Mccarthy K. D., Mehta T., Nicoll J. S., Tuominen M. T. and Lovley D. R. (2005) Extracellular electron transfer via microbial nanowires. *Nature* **435**, 1098–1101.

Rimstidt J. D. and Newcomb W. D. (1993) Measurement and analysis of rate data – the rate of reaction of ferric iron with pyrite. *Geochimica et Cosmochimica Acta* **57**, 1919–1934.

Roden E. E. (2003) Fe(III) oxide reactivity toward biological versus chemical reduction. *Environmental Science & Technology* **37**, 1319–1324.

Roden E. E. (2004) Analysis of long-term bacterial vs. chemical Fe(III) oxide reduction kinetics. *Geochimica et Cosmochimica Acta* **68**, 3205–3216.

Roden E. E. and Urrutia M. M. (1999) Ferrous iron removal promotes microbial reduction of crystalline iron(III) oxides. *Environmental Science & Technology* **33**, 1847–1853.

Roden E. E. and Urrutia M. M. (2002) Influence of biogenic Fe(II) on bacterial crystalline Fe(III) oxide reduction. *Geomicrobiology Journal* **19**, 209–251.

Roden E. E. and Zachara J. M. (1996) Microbial reduction of crystalline iron(III) oxides: influence of oxide surface area and potential for cell growth. *Environmental Science & Technology* **30**, 1618–1628.

Rosso K. M., Zachara J. M., Fredrickson J. K., Gorby Y. A. and Smith S. C. (2003) Nonlocal bacterial electron transfer to hematite surfaces. *Geochimica et Cosmochimica Acta* **67**, 1081–1087.

Royer R. A., Burgos W. D., Fisher A. S., Jeon B. H., Unz R. F. and Dempsey B. A. (2002a) Enhancement of hematite bioreduction by natural organic matter. *Environmental Science & Technology* **36**, 2897–2904.

Royer R. A., Burgos W. D., Fisher A. S., Unz R. F. and Dempsey B. A. (2002b) Enhancement of biological reduction of hematite by electron shuttling and Fe(II) complexation. *Environmental Science & Technology* **36**, 1939–1946.

Royer R. A., Dempsey B. A., Jeon B. H. and Burgos W. D. (2004) Inhibition of biological reductive dissolution of hematite by ferrous iron. *Environmental Science & Technology* **38**, 187–193.

Sall J., Creighton L. and Lehman A. (2005) *JMP Start Statistics: A Guide to Statistics and Data Analysis Using JMP and JMP IN Software*. Thomson Brooks/Cole, Pacific Grove, Calif.

Schwertmann U. (2003) *Iron Oxides: Structure, Properties, Reactions, Occurrences and Uses*. John Wiley and Sons Inc.

Schwertmann U. and Cornell R. M. (2000) *Iron Oxides in the Laboratory: Preparation and Characterization*. Wiley-VCH, Weinheim, New York.

Shi L., Chen B., Wang Z., Elias D. A., Mayer M. U., Gorby Y. A., Ni S., Lower B. H., Kennedy D. W., Wunschel D. S., Mottaz H. M., Marshall M. J., Hill E. A., Beliaev A. S., Zachara J. M., Fredrickson J. K. and Squier T. C. (2006) Isolation of a high-affinity functional protein complex between OmcA and MtrC: two outer membrane decaheme c-type cytochromes of *Shewanella oneidensis* MR-1. *Journal of Bacteriology* **188**, 4705–4714.

Sparks D. L. (2005) Toxic metals in the environment: the role of surfaces. *Elements* **1**, 193–197.

Stookey L. L. (1970) Ferrozine – a new spectrophotometric reagent for iron. *Analytical Chemistry* **42**, 779–781.

Stumm W. and Morgan J. J. (1996) *Aquatic Chemistry: Chemical Equilibria and Rates in Natural Waters*. Wiley, New York.

Tang R. K., Orme C. A. and Nancollas G. H. (2004) Dissolution of crystallites: surface energetic control and size effects. *ChemPhysChem.* **5**, 688–696.

Thompsen J. C. and Mottola H. A. (1984) Kinetics of the complexation of iron(II) with ferrozine. *Analytical Chemistry* **56**, 755–757.

Urrutia M. M., Roden E. E., Fredrickson J. K. and Zachara J. M. (1998) Microbial and surface chemistry controls on reduction of synthetic Fe(III) oxide minerals by the dissimilatory iron-reducing bacterium *Shewanella alga*. *Geomicrobiology Journal* **15**, 269–291.

Urrutia M. M., Roden E. E. and Zachara J. M. (1999) Influence of aqueous and solid-phase Fe(II) complexants on microbial reduction of crystalline iron(III) oxides. *Environmental Science & Technology* **33**, 4022–4028.

Von Canstein H., Ogawa J., Shimizu S. and Lloyd J. R. (2008) Secretion of flavins by Shewanella species and their role in extracellular electron transfer. *Applied and Environmental Microbiology* **74**, 615–623.

Wang C. Y., Bottcher C., Bahnemann D. W. and Dohrmann J. K. (2003) A comparative study of nanometer sized Fe(III)-doped TiO2 photocatalysts: synthesis, characterization and activity. *Journal of Materials Chemistry* **13**, 2322–2329.

Waychunas G. A., Kim C. S. and Banfield J. F. (2005) Nanoparticulate iron oxide minerals in soils and sediments: unique properties and contaminant scavenging mechanisms. *Journal of Nanoparticle Research* **7**, 409–433.

Xiong Y. J., Shi L., Chen B. W., Mayer M. U., Lower B. H., Londer Y., Bose S., Hochella M. F., Fredrickson J. K. and Squier T. C. (2006) High-affinity binding and direct electron transfer to solid metals by the *Shewanella oneidensis* MR-1 outer membrane c-type cytochrome OmcA. *Journal of the American Chemical Society* **128**, 13978–13979.

Yan B., Wrenn B. A., Basak S., Biswas P. and Giammar D. E. (2008) Microbial reduction of Fe(III) in hematite nanoparticles by *Geobacter sulfurreducens*. *Environmental Science & Technology* **42**, 6526–6531.

Yang C. C. and Jiang Q. (2006) Size effect on the bandgap of II–VI semiconductor nanocrystals. *Materials Science and Engineering B-Solid State Materials for Advanced Technology* **131**, 191–194.

Zachara J. M., Fredrickson J. K., Li S. M., Kennedy D. W., Smith S. C. and Gassman P. L. (1998) Bacterial reduction of crystalline Fe^{3+} oxides in single phase suspensions and subsurface materials. *American Mineralogist* **83**, 1426–1443.

Zachara J. M., Fredrickson J. K., Smith S. C. and Gassman P. L. (2001) Solubilization of Fe(III) oxide-bound trace metals by a dissimilatory Fe(III) reducing bacterium. *Geochimica et Cosmochimica Acta* **65**, 75–93.

Zachara J. M., Kukkadapu R. K., Fredrickson J. K., Gorby Y. A. and Smith S. C. (2002) Biomineralization of poorly crystalline Fe(III) oxides by dissimilatory metal reducing bacteria (DMRB). *Geomicrobiology Journal* **19**, 179–207.

Zhang H. Z., Penn R. L., Hamers R. J. and Banfield J. F. (1999) Enhanced adsorption of molecules on surfaces of nanocrystalline particles. *Journal of Physical Chemistry B* **103**, 4656–4662.

Associate editor: Johnson R. Haas